PS-wave moveout inversion for tilted transversely isotropic media: A physical-modeling study

Pawan Dewangan*, Ilya Tsvankin*, Mike Batzle†, Kasper van Wijk†, and Matt Haney**

* *Center for Wave Phenomena, Department of Geophysics, Colorado School of Mines, Golden, CO 80401-1887, USA*
† *Institute for Experimental Geophysics, Department of Geophysics, Colorado School of Mines, Golden, CO 80401-1887, USA*
** *Center for Wave Phenomena, Department of Geophysics, Colorado School of Mines, Golden, CO 80401-1887, USA (currently at Geophysical Technology Department, Sandia National Laboratories, Albuquerque, NM 87185-0750)*

ABSTRACT

Mode-converted PS-waves can provide critically important information for velocity analysis in transversely isotropic (TI) media. Here we demonstrate, with physical-modeling data, that the combination of long-spread reflection traveltimes of PP- and PS-waves can be inverted for the parameters of a horizontal TI layer with a tilted symmetry axis. The 2D multicomponent reflection data are acquired over a phenolic sample manufactured to simulate the effective medium formed by a system of steeply dipping, penny-shaped cracks.

The reflection moveout of PS-waves in this model is asymmetric, and the moveout-asymmetry attributes play a crucial role in constraining the TI parameters. Applying the modified PP+PS=SS method to the PP and PS traveltimes recorded in the symmetry-axis plane, we compute the time and offset asymmetry attributes of the PS-waves along with the traveltimes of the pure SS reflections. Then the algorithm of Dewangan and Tsvankin is used to invert the combination of the moveout attributes of the PP-, SS-, and PS-waves for the medium parameters and thickness of the sample.

Our estimates of the tilt of the symmetry axis and layer thickness almost coincide with the actual values. The inverted model was also validated by reproducing the results of transmission experiments with both P- and SV-wave sources. In particular, the transmitted SV wavefield exhibits a prominent cusp (triplication) accurately predicted by the parameter-estimation results.

Key words: multicomponent data, mode conversions, physical modeling, velocity analysis, anisotropic media

1 INTRODUCTION

Transverse isotropy (TI) is a common anisotropic symmetry usually associated with shaly sediments, fine layering on a scale small compared to seismic wavelength, or aligned penny-shaped cracks (e.g., Thomsen, 1986; Helbig, 1994). In active tectonic areas, such as fold-and-thrust belts, the symmetry axis of TI formations is often tilted away from the vertical. Such tilted transversely isotropic (TTI) models are typical for the Canadian Foothills where they cause significant mispositioning of imaged reflectors (e.g., Isaac and Lawton, 1999; Vestrum *et al.*, 1999). An effective TTI medium also describes a system of parallel, dipping, penny-shaped cracks embedded in isotropic host rock (Angerer *et al.*, 2002), as well as progradational sequences.

While conventional migration algorithms can be readily extended to handle transverse isotropy, parameter estimation for TTI media remains a challenging problem. In particular, Grechka and Tsvankin (2000) show that P-wave reflection moveout alone does not constrain the parameters of a horizontal TTI layer, even if a wide range of source-receiver azimuths is available. Furthermore, supplementing P-wave data with

wide-azimuth SV-wave traveltimes is still insufficient to make the inversion unique (Grechka and Tsvankin, 2000; Grechka *et al.*, 2002).

Important information for velocity analysis in TTI media is provided by mode-converted PS (PSV) data. Because of the deviation of the symmetry axis from both the vertical and horizontal directions, the moveout of PS-waves from horizontal reflectors becomes asymmetric (i.e., the PS-wave traveltime does not stay the same if the source and receiver are interchanged). As demonstrated by Dewangan and Tsvankin (2004a), moveout-asymmetry attributes of PS-waves can help to estimate all parameters of a horizontal TTI layer using solely reflection data. The algorithm of Dewangan and Tsvankin (2004a), based on a modification of the so-called "PP+PS=SS" method (Grechka and Tsvankin, 2002; Grechka and Dewangan, 2003), operates with long-offset PP and PS reflections acquired in the vertical plane that contains the symmetry axis (hereafter called the *symmetry-axis* plane).

Here, we show on physical-modeling data that the combination of PP and PS reflection traveltimes can indeed constrain all parameters of a horizontal TTI layer. Multicomponent, multioffset reflection seismic lines are acquired in the symmetry-axis plane of a phenolic sample to record long-spread moveouts of PP- and PS(PSV)-waves. Following the methodology of Dewangan and Tsvankin (2004a), the modified PP+PS=SS method is used to compute pure SS-wave reflection traveltimes and the asymmetry attributes of PS-waves. The moveout asymmetry information is then combined with the pure-mode (PP and SS) NMO velocities and zero-offset traveltimes to estimate the model parameters. The accuracy of the inverted TTI model is verified by matching the measured PP and PS traveltimes and reproducing the results of transmission experiments.

2 EXPERIMENTAL SETUP

To simulate a TTI layer, we used XX-paper-based phenolic composed of thin layers of paper bonded with phenolic resin. The effective medium due to this fine layering is anisotropic, and phenolic itself is known to have either TI or orthorhombic symmetry (Isaac and Lawton, 1999; Grechka *et al.*, 1999). The sample was prepared by cutting a large block of commercially available phenolic into smaller blocks and pasting them together at an angle to form a TTI medium. To simulate steeply dipping fractures similar to those identified by Angerer *et al.* (2002) on field data, the tilt ν of the symmetry axis from the vertical was chosen to be 70° (Figure 1).

The experiments were conducted in the Institute for Experimental Geophysics (IEG) at Colorado School of Mines (CSM). The measurements were made only in a vertical symmetry plane of the sample, where the velocities and polarizations are described by TI equations, even if the medium as a whole has orthorhombic symmetry. One reflection survey was acquired using source and receiver transducers (flat-faced cylindrical piezoelectric ultrasonic contact transducers). To generate P-waves, the source transducer was polarized vertically; shear (SV) waves were excited by a horizontal transducer.

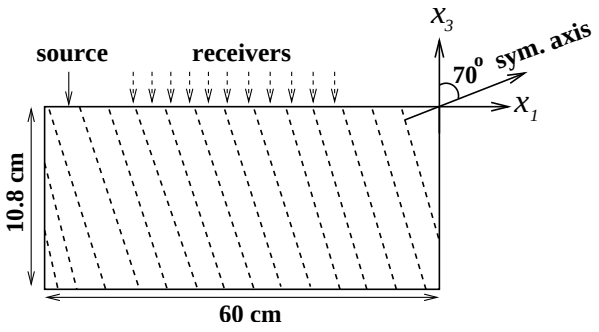

Figure 1. Physical model representing a horizontal TTI layer. The coordinate system is chosen in such a way that the symmetry axis is confined to the $[x_1, x_3]$-plane and is dipping in the negative x_1-direction. To simulate a reflection survey, the sources and receivers were placed on top of the sample in the symmetry-axis plane.

Another reflection data set was generated by the source transducer and recorded by a scanning laser vibrometer that measures the absolute particle velocity on the surface of the sample via the Doppler shift (Nishizawa *et al.*, 1997; Scales and van Wijk, 1999). The records of multiple shots were stacked to improve data quality. The scanning head is programmed to move the beam after each measurement, so that dense arrays of data can be recorded automatically. Therefore, data acquisition with the laser vibrometer is much more efficient compared with time-consuming transducer measurements, where relatively large receivers have to be moved manually.

3 SEISMIC REFLECTION EXPERIMENT

To study the moveout asymmetry of PS-waves and test the parameter-estimation methodology of Dewangan and Tsvankin (2004a), we acquired a multioffset 2D reflection survey in the symmetry-axis plane, as described above. The inversion algorithm operates on common-midpoint (CMP) gathers of PP- and PS-waves and requires the offset-to-depth ratio to reach at least two. Since recording a CMP gather involves moving both the source and receiver transducers, it is cumbersome and prone to error in positioning. Instead, we decided to collect shot gathers (Figure 1) and interpret them as CMP gathers, which is valid for laterally homogeneous media.

To verify that the lateral heterogeneity of the sample is negligible, we recorded a constant-offset P-wave section (Figure 2). The first arrival (the direct P-wave)

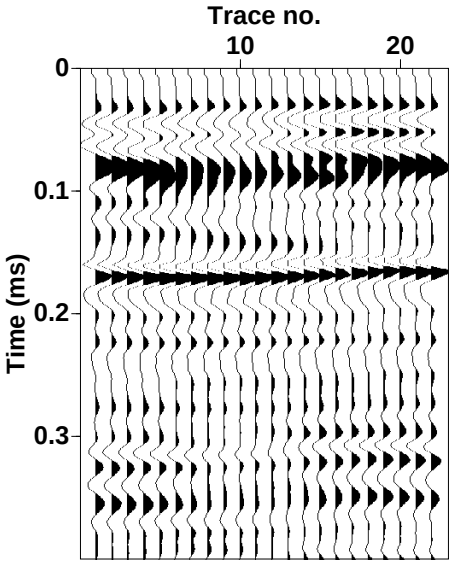

Figure 2. Constant-offset P-wave section acquired to validate the assumption of lateral homogeneity.

and the P-wave multiple at a time of about 0.17 ms exhibit relatively weak traveltime and waveform variations along the line. The waveform of the P-wave primary recorded around 0.08 ms is distorted because of its interference with the ground roll. The minor lateral variations in the waveforms may also be related to errors in receiver positioning and to scattering on air bubbles between imperfectly glued blocks.

Shot gathers of PP- and PS-waves were recorded by fixing the P-wave shot transducer at one end of the model and manually moving the receiver transducer with an increment of 1 cm until the offset reached 30 cm, which corresponds to an offset-to-depth ratio of 2.8 (Figure 1). The whole procedure was repeated by placing the source transducer at the other end of the model to record negative offsets. The traces for positive and negative offsets were then combined to form a split-spread CMP gather.

Another independent data set was obtained by replacing the receiver transducer with the laser vibrometer. The sampling interval for the vibrometer dataset was 2 mm; the maximum offset-to-depth ratio was limited to 2.5 (the maximum offset was 27 cm).

3.1 Vertical component (PP-waves)

For the vertical wavefield component recorded with the contact transducer (Figure 3a), the offset could not be smaller than 3 cm because of the finite transducer size. The minimum offset for the densely spaced data recorded with the laser vibrometer was 2 cm (Figure 3b). Since the vibrometer measures the vertical velocity at a point, it is possible to record closer to the source but the signal quality deteriorates at far offsets.

The two data sets in Figure 3 are quite similar, but identification of reflection events is hampered by their interference with the ground roll. To suppress the ground roll, we applied standard F-K dip filtering that significantly improved the quality of the section (Figure 4). The first arrival is the direct P-wave traveling with the horizontal velocity close to 2620 m/s. The strong ground roll clearly visible in Figure 3 travels with a velocity of 1285 m/s, which is slightly smaller than the shear-wave velocity along the symmetry axis. The P-wave primary reflection from the bottom of the block and the first multiple can be identified at zero-offset times of 0.064 ms and 0.128 ms, respectively. Since the laser dataset is more densely sampled and has better coherency, we used it for manually picking the traveltimes of the primary reflection.

The dominant frequency of the P-wave data decreases from 200 kHz at near offsets to around 40 kHz at far offsets, which indicates that the medium is strongly attenuative (Figure 5). Assuming a dominant frequency of 100 kHz, the units of time and distance used in our experiment should be scaled (multiplied) by 5000 to obtain the corresponding values for seismic field data with a frequency of 20 Hz; the equivalent thickness of the layer would be 540 m.

To estimate the P-wave normal moveout (NMO) velocity, we applied conventional hyperbolic velocity analysis (Figure 6). The influence of nonhyperbolic moveout was mitigated by muting out long offsets. The maximum offset-to-depth ratio used to compute the semblance in Figure 6a was close to one. The best-fit NMO velocity $V_{\mathrm{nmo},P}$, which flattens the near-offset primary and multiple reflections (Figure 6b), is 2350±50 m/s.

At large offsets, the NMO-corrected gather in Figure 6b is not flat, which indicates that the moveout curve is nonhyperbolic. This deviation from hyperbolic moveout in a single homogeneous layer indicates that the medium is anisotropic, and the anisotropy is not elliptical (e.g., Tsvankin, 2001).

The event arriving at $t_0 = 0.11$ ms with a lower moveout velocity than that of the P-waves may be interpreted as a converted PS mode. Since the PS-wave polarization vector at small and moderate offsets is close to the horizontal plane, this event is not prominent on the vertical component. To clearly identify mode-converted waves and pick their traveltimes, we recorded the horizontal component of the wavefield, as described in the next section.

3.2 Horizontal component (PS-waves)

The horizontal wavefield component from the vertical source was recorded with the same settings as the ver-

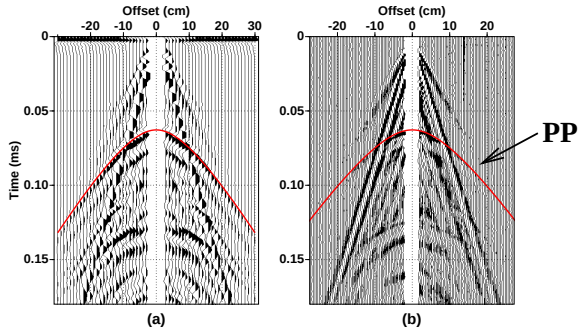

Figure 3. Vertical component of the wavefield. (a) Data recorded with the P-wave contact transducers; (b) densely sampled data recorded with the laser vibrometer. The first arrival is the direct P-wave; the PP-wave reflection from the bottom of the block (solid line) arrives at a zero-offset time of 0.064 ms.

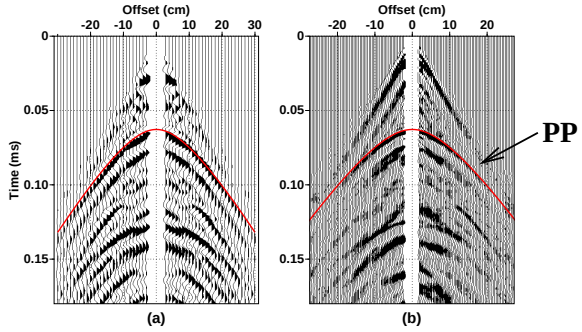

Figure 4. Data from Figure 3 after application of F-K filtering to suppress the ground roll.

tical component. The receiver transducer was oriented horizontally in the symmetry-axis plane to record mode-converted PS(PSV)-waves (Figure 7a). We verified that there was almost no energy on the crossline (transverse) component, which indicates that the data were indeed acquired in a symmetry plane of the medium. Also, shear-wave splitting along the symmetry axis was negligible, suggesting that the model is either TI or a special case of orthorhombic media with equal anisotropy coefficients $\gamma^{(1)}$ and $\gamma^{(2)}$ (Tsvankin, 1997, 2001). Because of the kinematic equivalence between the symmetry planes of orthorhombic and TI media, the parameter-estimation algorithm of Dewangan and Tsvankin (2004a) is valid for both plausible models.

So far, the laser vibrometer system available at CSM has not been used to record the horizontal component of the wavefield. This limitation, however, can be overcome by recording mode-converted SP-waves and treating their traveltimes (according to reciprocity) as those of the corresponding PS-waves. Instead of the P-wave transducer used before, a shear transducer served

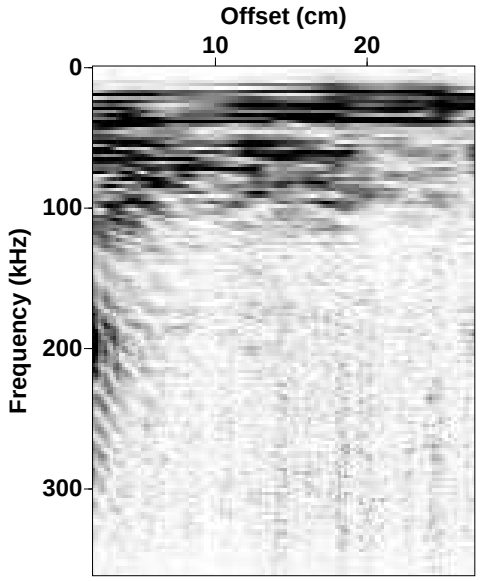

Figure 5. Amplitude spectra of the P-wave traces showing a decrease in frequency with offset.

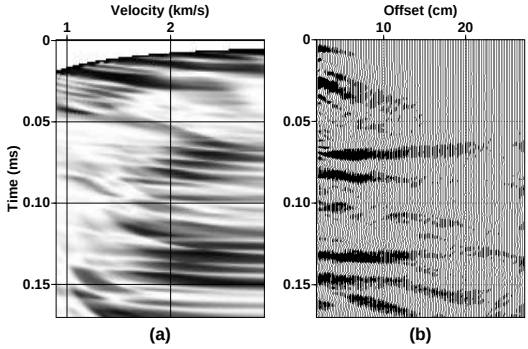

Figure 6. Conventional hyperbolic velocity analysis of the P-wave data. (a) Semblance panel computed for the maximum offset-to-depth ratio close to one; (b) the gather corrected for hyperbolic moveout using a moveout velocity of 2350 m/s.

as the source and the laser vibrometer as the detector of the vertical wavefield component (Figure 7b). In the moveout analysis below, the traveltimes of the acquired SP-wave were substituted for those of the PS-wave, while the sign of the SP-wave source-receiver offset was reversed when constructing a split-spread PS-wave gather.

Both acquired sections after application of F-K filtering are displayed in Figure 8. As was the case with the vertical component, there is close similarity between

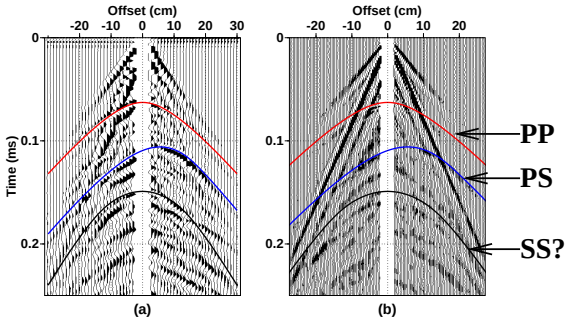

Figure 7. Horizontal component of the wavefield. Data recorded with: (a) the P-wave source transducer and S-wave receiver transducer; (b) the S-wave source transducer and the laser vibrometer as the receiver. The converted wave from the bottom of the model has an asymmetric moveout curve with the apex at 0.11 ms. The solid lines are the picked traveltimes of the PP, PS, and SS arrivals.

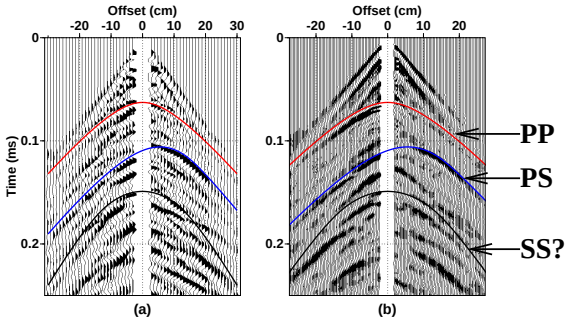

Figure 8. Data from Figure 7 after application of F-K filtering to suppress the ground roll. Negative offsets are displayed in reverse polarity to facilitate picking of PS traveltimes.

the two data sets recorded using different experimental setups. The moveout of the mode-converted PS- and SP-waves is strongly asymmetric, with a substantial difference between the traveltimes for positive and negative offsets. Since the model is laterally homogeneous, the PS-wave moveout asymmetry is caused entirely by the oblique orientation of the symmetry axis. Note that the moveout of converted waves is symmetric in any laterally homogeneous medium with a horizontal symmetry plane, including TI models with a vertical (VTI) and horizontal (HTI) symmetry axis (Grechka and Tsvankin, 2000; Dewangan and Tsvankin, 2004a).

The traveltime picks of the PS-wave, marked by the solid line in Figure 8, were made using the laser vibrometer dataset. Due to the moveout asymmetry, the minimum PS-wave traveltime is recorded at an offset of x=6 cm where the wavelet reverses its polarity. To facilitate visual correlation of PS traveltimes, we removed this polarity reversal from the sections in Figure 8.

The PP-wave primary reflection can be identified even on the horizontal component around the zero-offset time $t_{P0} = 0.064$ ms. It may also be possible to tentatively pick the SS-wave reflected arrival but, as expected, in Figure 8 it is much weaker than the converted modes.

3.3 Data processing

The key processing step was application of the PP+PS=SS method (Grechka and Tsvankin, 2002; Grechka and Dewangan, 2003) to compute the traveltimes of the pure SS (SVSV) reflections from the PP and PS data. The reflection traveltimes of both the PP-waves (on the vertical component) and the converted waves (on the horizontal component) were manually picked from the laser vibrometer dataset. To smooth the traveltimes and interpolate/extrapolate them at near offsets, we fitted a six-order polynomial to both PP and PS moveouts using the least-squares method.

The idea of the PP+PS=SS method is to identify two "reciprocal" PS-wave rays with the same reflection (conversion) point and combine their traveltimes with that of the PP-wave to compute the moveout of the SS-wave primary reflection. This can be accomplished by matching the reflection slopes on common-receiver gathers of PP- and PS-waves, as illustrated in Figure 9 (Grechka and Tsvankin, 2002). Since the PS rays recorded at points $x^{(3)}$ and $x^{(4)}$ have the same reflection point as the PP reflection $x^{(1)}Rx^{(2)}$, the traveltime τ_{SS} of the SS-wave (not physically excited in the survey) is determined from

$$\begin{aligned}\tau_{SS}(x^{(3)},x^{(4)}) &= t_{PS}(x^{(1)},x^{(3)}) + t_{PS}(x^{(2)},x^{(4)}) \\ &- t_{PP}(x^{(1)},x^{(2)}),\end{aligned} \tag{1}$$

where t_{PS} and t_{PP} are the traveltimes of the PS and PP reflections, respectively. Note that application of this technique requires correlating PP and PS reflection events and picking their traveltimes, although explicit velocity information is not needed.

Alternatively, PP and PS arrivals with the same reflection point can be found by computing the time τ_{SS} in equation (1) for each desired SS-wave shot-receiver pair $(x^{(3)},x^{(4)})$ and a wide range of the coordinates ($x^{(1)}$ and $x^{(2)}$) (Grechka and Dewangan, 2003; Dewangan and Tsvankin, 2004a):

$$\begin{aligned}\tau_{SS}(x^{(3)},x^{(4)}) = \min_{x^{(1)},\,x^{(2)}} \Big(&t_{PS}(x^{(1)},x^{(3)}) \\ &+ t_{PS}(x^{(2)},x^{(4)}) - t_{PP}(x^{(1)},x^{(2)})\Big).\end{aligned} \tag{2}$$

The minimum of the function (2) in both the $x^{(1)}$ and $x^{(2)}$ directions allows us to identify the P-wave sources that generate the reciprocal PS arrivals with the same reflection point. The value of τ_{SS} corresponding to this minimum yields the SS traveltime from ($x^{(3)}$ to $x^{(4)}$).

We opted to apply the latter procedure to compute

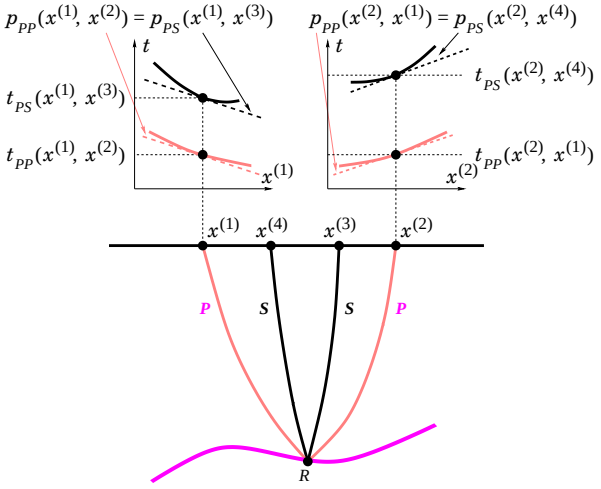

Figure 9. PP+PS=SS method is designed to find the source/receiver coordinates of the PP and PS rays with the same (albeit unknown) reflection point R. By matching the slopes on common-receiver gathers (i.e., the ray parameters) of the PP- and PS-waves, the method estimates the recording locations $x^{(3)}$ and $x^{(4)}$ of the PS arrivals that have the common P-wave legs with the PP reflection from $x^{(1)}$ to $x^{(2)}$ (after Grechka and Tsvankin, 2002).

the SS-wave traveltime as a function of the SS-wave offset $x_{SS} = |x^{(3)} - x^{(4)}|$ (Figure 10). Then, conventional hyperbolic velocity analysis was applied to the constructed SS arrivals to estimate their stacking velocity ($V_{\mathrm{nmo},S} \approx 1780$ m/s) and zero-offset traveltime ($t_{S0} \approx 0.149$ ms).

Next, we followed the methodology of Dewangan and Tsvankin (2004a) in computing the time and offset asymmetry attributes of the PS-wave:

$$\Delta t_{PS}(x^{(3)}, x^{(4)}) = t_{PS}(x^{(1)}, x^{(3)}) - t_{PS}(x^{(2)}, x^{(4)}); \quad (3)$$

$$\Delta x_{PS}(x^{(3)}, x^{(4)}) = |x_{PS}(x^{(1)}, x^{(3)})| - |x_{PS}(x^{(2)}, x^{(4)})|. \quad (4)$$

The time asymmetry factor Δt_{PS} (Figure 11a) rapidly increases with offset and reaches about 20% of the zero-offset time. In contrast, the depth-normalized offset asymmetry Δx_{PS} reaches its maximum (by absolute value) at small SS-wave offsets (Figure 11b), as predicted by the analytic results of Dewangan and Tsvankin (2004a) for the symmetry axis deviating by more than 45° from the vertical. Note that the factor Δx_{PS} at zero offset ($x^{(3)} = x^{(4)}$) is twice the offset $x_{\min}$ corresponding to the minimum traveltime in the PS-wave CMP gather (Tsvankin and Grechka, 2000).

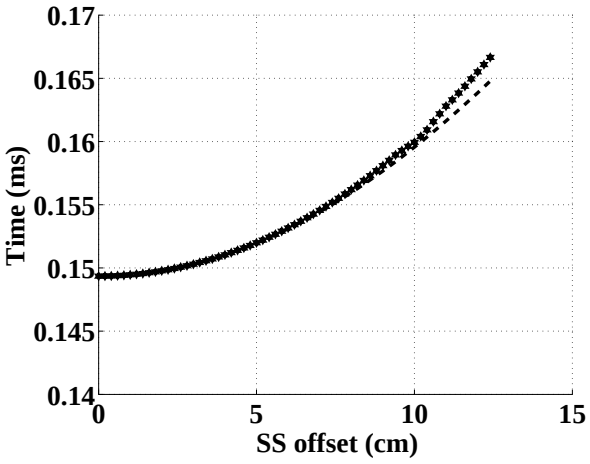

Figure 10. SS-wave traveltime computed using the PP+PS=SS method (stars) as a function of the SS-wave offset. The dashed line corresponds to the best-fit hyperbola with a moveout velocity of 1780 m/s.

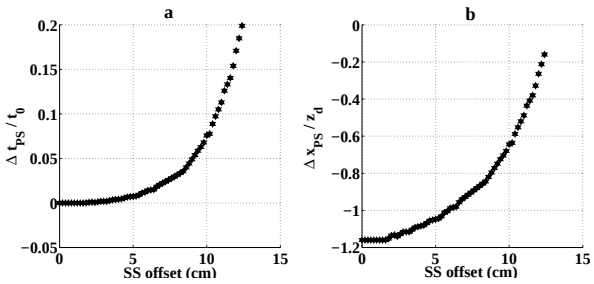

Figure 11. Moveout-asymmetry attributes of the PS-wave computed from equations (3) and (4). (a) The time asymmetry Δt_{PS} normalized by the zero-offset PS-wave time; (b) the corresponding offset asymmetry Δx_{PS} normalized by the layer thickness.

3.4 Parameter Estimation

The vector $\boldsymbol{d}$ of input data for the inversion procedure includes the NMO velocities and zero-offset times of the PP- and SS-waves and the asymmetry attributes of the PS-wave:

$$\boldsymbol{d} \equiv \left\{ V_{\mathrm{nmo},P}\,,\, t_{P0}\,,\, V_{\mathrm{nmo},S}\,,\, t_{S0}\,,\, \Delta t_{PS}(x_{SS})\,,\, \Delta x_{PS}(x_{SS}) \right\}, \quad (5)$$

The analytic expressions needed to model these quantities are given in Dewangan and Tsvankin (2004a), who used the offset $x_{\min}$ of the traveltime minimum instead of the asymmetry factor Δx_{PS}. Here, however, we prefer to operate with the function (array) $\Delta x_{PS}(x_{SS})$ that helps to obtain more accurate param-

eter estimates in the presence of noise (Dewangan and Tsvankin, 2004b).

The model vector $\boldsymbol{m}$ includes the five relevant TTI parameters and the layer thickness z:

$$\boldsymbol{m} \equiv \Big\{ V_{P0}\,,\, V_{S0}\,,\, \epsilon\,,\, \delta\,,\, \nu,\, z \Big\}, \tag{6}$$

where V_{P0} and V_{S0} are the velocities of P- and S-waves (respectively) in the symmetry direction, ϵ and δ are Thomsen anisotropy parameters, and ν (tilt) is the angle between the symmetry axis and the verical. To estimate the elements of $\boldsymbol{m}$, we applied the nonlinear inversion algorithm discussed in Dewangan and Tsvankin (2004a), with the misfit (objective) function given by

$$\begin{aligned}\mathcal{F} \equiv & \frac{(V^{\rm calc}_{{\rm nmo},P} - V^{\rm meas}_{{\rm nmo},P})^2}{(V^{\rm meas}_{{\rm nmo},P})^2} + \frac{(V^{\rm calc}_{{\rm nmo},S} - V^{\rm meas}_{{\rm nmo},S})^2}{(V^{\rm meas}_{{\rm nmo},S})^2} \\ & + \frac{(t^{\rm calc}_{P0} - t^{\rm meas}_{P0})^2}{(t^{\rm meas}_{P0})^2} + \frac{(t^{\rm calc}_{S0} - t^{\rm meas}_{S0})^2}{(t^{\rm meas}_{S0})^2} \\ & + \frac{\sum_0^{x^{\rm max}_{SS}} (\Delta t^{\rm calc}_{PS} - \Delta t^{\rm meas}_{PS})^2}{(\sum_0^{x^{\rm max}_{SS}} \Delta t^{\rm meas}_{PS})^2} \\ & + \frac{\sum_0^{x^{\rm max}_{SS}} (\Delta x^{\rm calc}_{PS} - \Delta x^{\rm meas}_{PS})^2}{(\sum_0^{x^{\rm max}_{SS}} \Delta x^{\rm meas}_{PS})^2}\,. \end{aligned} \tag{7}$$

Here, the superscripts "calc" and "meas" denote the calculated and measured quantities (respectively), and $x^{\rm max}_{SS}$ is the maximum offset of the constructed SS-wave that corresponds to the offset-to-depth ratio of the recorded PP data close to two.

The initial guesses for the vertical velocities and anisotropy coefficients were based on the isotropic relationships,

$$\begin{aligned} & V_{P0} = V_{{\rm nmo},P} = 2.35\,{\rm km/s}\,,\, V_{S0} = V_{{\rm nmo},S} = 1.78\,{\rm km/s}, \\ & \epsilon = 0,\, \delta = 0,\, z = V_{{\rm nmo},P}\, t_{P0}/2 = 7.52\,{\rm cm}\,. \end{aligned} \tag{8}$$

The initial tilt of the symmetry axis was randomly chosen between 50° and 85°. Although both the tilt ν and thickness z were known, they were estimated from the data to simulate a field experiment.

To assess the stability of the inversion, the algorithm was applied to multiple realizations of the input PP and PS traveltimes contaminated by random Gaussian noise with zero mean. The standard deviation of the noise was equal to 1/8 of the dominant period, which was assumed to be close to the accuracy of the traveltime picking. The inversion results for 200 realizations of the Gaussian noise are shown in Figure 12. The best-constrained parameter combination is the difference between ϵ and δ, which controls both the time and offset asymmetry (Dewangan and Tsvankin, 2004a). Note that the sample is strongly anisotropic, with the value of ϵ approaching 50%.

The PP- and PS-wave traveltimes computed for the estimated model are practically indistinguishable from the picked traveltimes at all offsets (Figures 4 and 8). Another indication of the high accuracy of the inversion procedure is that the errors in the known values of ν and z are almost negligible.

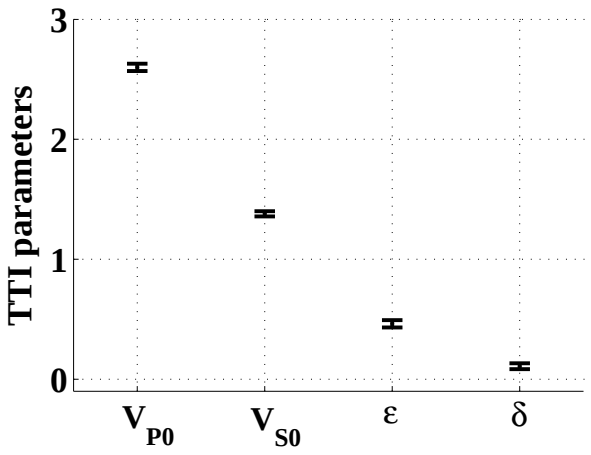

Figure 12. Thomsen parameters of the sample estimated from 2D PP and PS data in the symmetry-axis plane (the velocities are in km/s). The mean values are $V_{P0} = 2.6$ km/s, $V_{S0} = 1.38$ km/s, $\epsilon = 0.46$, and $\delta = 0.11$. The estimated tilt of the symmetry axis and layer thickness (not shown) are $\nu = 70°$ and $z = 10.9$ cm. The error bars correspond to the following standard deviations in each parameter: 2% for V_{P0}, V_{S0}, and z, 0.03 for ϵ and δ, and 1° for ν.

4 TRANSMISSION/CALIBRATION EXPERIMENT

To verify the estimated model using an independent data set, we conducted a transmission experiment on the same sample. The P-wave source transducer was fixed at the bottom of the model, while the laser vibrometer scanned the top with a regular interval of 2 mm. The experiment was set up in such a way that the first-arrival traveltime could be measured for the full range of propagation angles ($0° - 90°$) from the symmetry axis.

It is believed that laboratory experiments employing transducers of relatively large size may yield measurements of phase, not group velocity (Dellinger and Vernik, 1994). Our transducer, however, was small (15 mm) compared to the thickness of the model (108 mm), so the traveltimes should be determined by the corresponding group velocities. Therefore, to reproduce the results of the transmission experiment, we computed the group velocity V_G and the group angle ϕ for the inverted model using the standard TI equations (e.g., Tsvankin, 2001):

$$V_G = V \sqrt{1 + \Big(\frac{1}{V}\,\frac{dV}{d\theta}\Big)^2}\;; \tag{9}$$

$$\tan\phi = \frac{\tan\theta + \frac{1}{V}\frac{dV}{d\theta}}{1 - \frac{\tan\theta}{V}\frac{dV}{d\theta}}\ , \tag{10}$$

where V and θ are the phase velocity and phase angle. It was assumed that ray bending was negligible, and the group angle ϕ corresponds to the source-receiver line.

Figure 13 shows the raw transmission data, with the zero- and far-offset receiver positions corresponding to the directions approximately perpendicular and parallel (respectively) to the symmetry axis. The first break is the direct P-wave followed by the relatively weak direct S-wave. The solid line marks the P-wave arrival time computed for the inverted TTI model using equations (9) and (10). Evidently, the estimated model parameters accurately predict the P-wave velocity in the transmission experiment that includes a wider range of propagation directions compared to the reflection data set.

It is interesting that the wavefront of the direct S-wave arrival in Figure 13 exhibits a cusp (triplication) at oblique angles with the symmetry axis. The existence and size of the cusp is mostly governed by the magnitude of the anisotropic parameter $\sigma \equiv (V_{P0}/V_{S0})^2\,(\epsilon-\delta)$ (Tsvankin, 2001; Thomsen, 2002) that reaches 1.24 for our model. While SV-wave cusps in TI media are well understood theoretically, their experimental observations are rare (e.g., Slater *et al.*, 1993).

To identify the cusp more clearly and measure the transmitted shear-wave traveltimes, we performed another transmission experiment, this time with the S-wave transducer as the source (Figure 14b). The transmitted wavefield was also computed (Figure 14a) for the inverted TTI model from Figure 12 using the spectral-element method (Komatitsch and Vilotte, 1998). Although the spectral-element code is 2D and cannot be expected to accurately reproduce the recorded amplitudes, the agreement between the measured and modeled wavefields in Figure 14 is excellent.

The spatial extent of the cusp in Figure 14 is significantly larger than that predicted by the group-velocity surface (i.e., by ray-theory modeling). This is consistent with the observation by Martynov and Mikhailenko (1984) that ray theory underestimates the actual size of the SV-wave cusp in TI media computed by solving the wave equation. The reflected PS data analyzed above do not exhibit cuspoidal behavior because the shear-wave group angles corresponding to the cusp are not reached during the P-to-S conversion at the bottom of the layer.

The ray-theoretical S-wave traveltimes computed for the inverted model (solid lines) match the observed arrivals only up to an offset of about 10 cm. To explain the discrepancy at larger offsets, we increased the frequency of the signal used in the spectral-element modeling (Figure 15). The higher-frequency wavefield shows two distinct arrivals with close traveltimes – the direct S-wave and the refracted P-wave. The interference of these waves on the lower-frequency section (Figure 14) produces a complicated wavelet that arrives ahead of the direct shear wave at large offsets. Another wave more clearly visible in Figure 15 is the P-wave multiple in the layer.

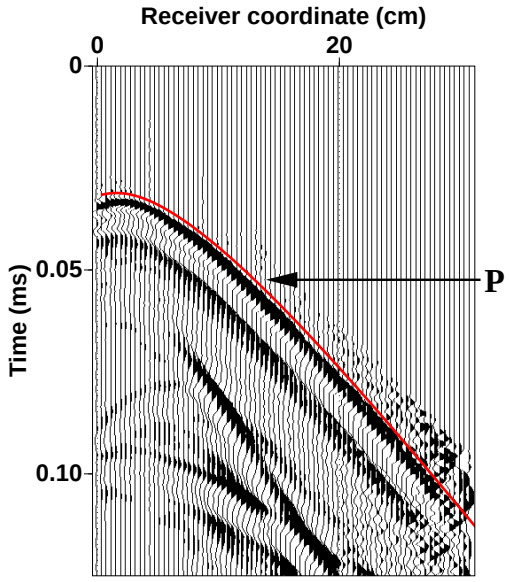

Figure 13. Transmitted wavefield excited by the P-wave transducer and recorded by the laser vibrometer at the top of the model. The solid line is the P-wave traveltime modeled using the inverted parameters from Figure 12.

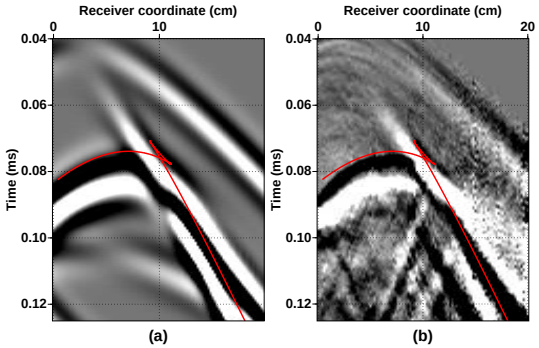

Figure 14. Shear-wave cusp in the transmitted wavefield excited by the S-wave transducer. (a) The wavefield simulated with the spectral element method; (b) the wavefield recorded by the laser vibrometer. The solid line is the S-wave traveltime computed from the group-velocity surface for the inverted model in Figure 12.

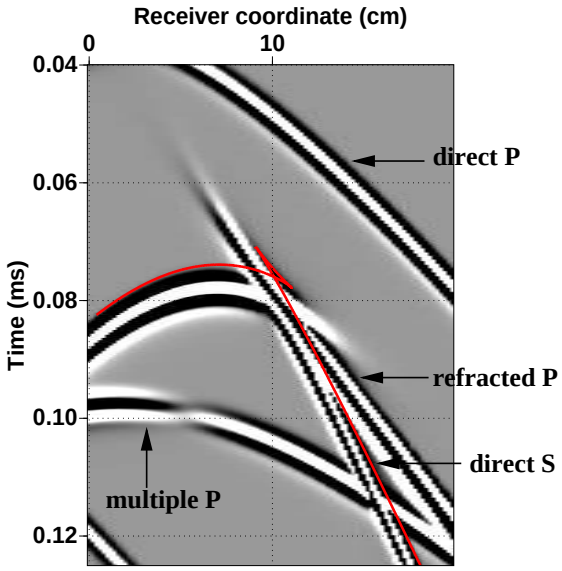

Figure 15. Same as Figure 14a, but the spectral-element modeling was performed with a higher-frequency wavelet.

5 DISCUSSION AND CONCLUSIONS

To estimate the anisotropic parameters of tilted TI media, P-wave reflection moveout can be combined with converted PS-waves. Here, we used 2D physical-modeling reflection data recorded over a horizontal layer of phenolic material to demonstrate that long-spread PP and PS (PSV) reflection traveltimes can be inverted in a stable way for the orientation of the symmetry axis and the pertinent Thomsen parameters. The large tilt of the symmetry axis from the vertical (70°) was designed to model the effective medium due to a system of steeply dipping, parallel cracks.

The data were acquired in the plane that contains the symmetry axis of the material (the "symmetry-axis plane") and processed using the modified version of the PP+PS=SS method developed by Dewangan and Tsvankin (2004a). In addition to the traveltimes of the pure SS reflections (which are not physically excited in the survey), this methodology produces the moveout-asymmetry attributes of the recorded PS arrivals. Our case study confirmed the conclusion of Dewangan and Tsvankin (2004a) that the combination of the PS-wave time and offset asymmetry factors with the NMO velocities and zero-offset times of the PP- and SS-waves makes it possible to estimate the medium parameters and layer thickness. Note that in field experiments the azimuth of the symmetry axis has to be estimated from the polarization of PS-waves or the azimuthal variation of such signatures as NMO velocities and AVO (amplitude variation with offset) gradients.

The sample proved to be strongly anisotropic, with the magnitude of P-wave velocity variations approaching 50% ($\epsilon = 0.46$, $\delta = 0.11$). The inversion algorithm provided accurate estimates of the known values of the tilt of the symmetry axis and the layer thickness. Still, to verify the parameter-estimation results, we conducted a transmission experiment using both P-wave and S-wave transducers. The P-wave group-velocity curve computed for the inverted model accurately matched the first breaks of the transmitted P-wave.

The wavefront of the transmitted SV-wave has a more complicated shape, with a cusp (triplication) between the symmetry axis and the isotropy plane. Although the observed cusp is noticeably wider than that predicted by the group-velocity surface calculated for the estimated model, this discrepancy is caused by the inadequacy of ray theory in describing triplications. More accurate modeling using the spectral-element method allowed us to reproduce the cusp and all other major features of the transmitted wavefield excited by the shear transducer. Since the shape and spatial extent of SV-wave cusps are highly sensitive to the medium parameters, the excellent agreement between the modeling results and recorded wavefield confirms the robustness of our inversion method.

6 ACKNOWLEDGMENTS

We are grateful to members of the A(nisotropy)-Team of the Center for Wave Phenomena (CWP), Colorado School of Mines (CSM), for helpful discussions and to Ken Larner (CSM) for his careful review of the manuscript. The support for this work was provided by the Consortium Project on Seismic Inverse Methods for Complex Structures at CWP and by the Chemical Sciences, Geosciences and Biosciences Division, Office of Basic Energy Sciences, U.S. Department of Energy. The experimental work was supported by the National Science Foundation (EAR-0111804, EAR-0337379) and the Army Research Office (DAAG55-98-1-0277, DAAD19-03-1-0292).

REFERENCES

Angerer, E., Horne, S. A., Gaiser, J. E., Walters, R., Bagala, S. and Vetri, L., 2002, Characterization of dipping fractures using PS mode-converted data: 72th Annual International Meeting, Society of Exploration Geophysicists, Expanded Abstracts, 1010–1013.

Bakulin, A., Grechka, V., and Tsvankin, I., 2000, Estimation of fracture parameters from reflection seismic data – Part I: HTI model due to a single fracture set: Geophysics, **65**, 1788–1802.

Dellinger, J. and Vernick, L., 1994, Do traveltimes in

pulse-transmission experiments yield anisotropic group or phase velocities?: Geophysics, **59**, 1774–1779.

Dewangan, P., and Tsvankin, I. 2004a, Application of PS-wave moveout asymmetry in parameter estimation for tilted TI media – Part I: Horizontal TTI layer: Geophysics, under review.

Dewangan, P., and Tsvankin, I. 2004b, Application of PS-wave moveout asymmetry in parameter estimation for tilted TI media – Part II: Dipping TTI layer: Geophysics, under review.

Grechka, V., and Dewangan, P., 2003, Generation and processing of pseudo shear-wave data: Theory and case study: Geophysics, **68**, 1807–1816.

Grechka, V., Pech, A., and Tsvankin, I., 2002, Multicomponent stacking-velocity tomography for transversely isotropic media: Geophysics, **67**, 1564–1574.

Grechka, V., Theophanis, S. and Tsvankin, I., 1999, Joint inversion of P- and PS-waves in orthorhombic media: Theory and a physical modeling study: Geophysics, **64**, 146–161.

Grechka, V., and Tsvankin, I., 2000, Inversion of azimuthally dependent NMO velocity in transversely isotropic media with a tilted axis of symmetry: Geophysics, **65**, 232–246.

Grechka, V., and Tsvankin, I., 2002, PP+PS=SS: Geophysics, **67**, 1961–1971.

Helbig, K., 1994, Foundations of elastic anisotropy for exploration seismics: Pergamon Press.

Isaac, J. H., and Lawton, D. C., 1999, Image mispositioning due to dipping TI media: A physical seismic modeling study: Geophysics, **64**, 1230–1238.

Komatitsch, D., and Vilotte, J. P., 1998, The spectral-element method: An efficient tool to simulate the seismic response of 2D and 3D geological structures: Bulletin of the Seismological Society of America, **88**, 368–392.

Martynov, V. N., and Mikhailenko, B.G., 1984, Numerical modelling of elastic waves in anisotropic inhomogeneous media for the halfspace and the sphere: Geophysical Journal of the Royal Astronomical Society, **76**, 53–63.

Nishizawa O., Satoh, T., Lei, X., and Kuwahara, Y., 1997, Laboratory studies of seismic wave propagation in inhomogeneous media using a laser doppler vibrometer: Bulletin of the Seismological Society of America, **87**, 809–823.

Scales, J. A., and van Wijk, K., 1999, Multiple scattering attenuation and anisotropy of ultrasonic surface waves: Applied Physics Letters, **74**, 3899–3901.

Slater, C., Crampin, S., Brodov, L. Yu., and Kuznetsov, V. M., 1993, Observations of anisotropic cusps in transversely isotropic clay: Canadian Journal of Exploration Geophysics, **29**, 216–226.

Thomsen, L., 1986, Weak elastic anisotropy: Geophysics, **51**, 1954–1966.

Thomsen, L., 2002, Underst anding seismic anisotropy in exploration and exploitation: DISC (Distinuguished Instructor Short Course) Notes, Society of Exploration Geophysicists.

Tsvankin, I., 1997, Reflection moveout and parameter estimation for horizontal transverse isotropy: Geophysics, **62**, 614–629.

Tsvankin, I., 2001, Seismic signatures and analysis of reflection data in anisotropic media: Elsevier Science Publ. Co., Inc.

Tsvankin, I., and Grechka, V., 2000, Dip moveout of converted waves and parameter estimation in transversely isotropic media: Geophysical Prospecting, **48**, 257–292.

Vestrum, R. W., Lawton, D. C., and Schmid, R., 1999, Imaging structures below dipping TI media: Geophysics, **64**, 1239–1246.